Fabrication of Sensitive High-Temperature Superconducting Bolometers on a Yttria-Stabilized Zirconia Membrane

by

Ann Satoko Hirahara

Submitted to the Department of
Materials Science and Engineering
in Partial Fulfillment of
the Requirements for the Degree of

MASTER OF SCIENCE

at the

Massachusetts Institute of Technology

June 1995

Signature of Author.....
Department of Materials Science and Engineering
12 May 1995

Certified by.....
Professor Michael Cima
Thesis Advisor

Accepted by.....
Carl V. Thompson II
Professor of Electronic Materials
Chair, Departmental Committee on Graduate Students

Fabrication of Sensitive High-Temperature Superconducting Bolometers on a Yttria-Stabilized Zirconia Membrane

by

Ann Satoko Hirahara

Submitted to the Department of Materials Science and Engineering
on 12 May 1995 in partial fulfillment of the
requirements for the Degree of Master of Science in
Materials Science and Engineering

Abstract

High temperature superconducting bolometers have the potential to match the performance of HgCdTe infrared detectors at wavelengths greater than 15 μm, where the density of photo-generated carriers in the semiconductor drops significantly, thus reducing the detector's sensitivity. A novel thin-film processing technique involving a sacrifical etching step was developed to fabricate array-compatible YBCO bolometers on free-standing yttria-stabilized zirconia (YSZ) membranes. The 50 x 50 μm^2 YSZ membranes were about 1500 Å thick, supported by four thin legs with aspect ratios varying from 5 to 20 squares. The thermal conductance to the substrate (G) was measured to be as low as 6×10^{-7} W/K. A single superconducting line on the membrane served as the thermometer, with one lead on each of the four legs. Issues such as thin film stress and chemical reaction during the deposition of the multilayer films, as well as the prevention of damage to the superconducting oxide during processing were addressed during the development of the fabrication process. YBCO bolometers on free-standing YSZ membranes were successfully fabricated, and devices with optical noise equivalent powers (NEP's) as low as 1.5×10^{-12} W/√Hz were achieved.[14] This value not only matches the lowest reported NEP for a superconducting bolometer[13], but the device also has a time constant that is about 50 times faster.

Thesis Supervisor: Dr. Michael J. Cima

Title: Professor of Ceramics Processing

Table of Contents

List of Figures....4
List of Tables....5
Acknowledgments....6
1. Background....7
1.1 Introduction....7
1.2 Structure and Properties of $YBa_2Cu_3O_{7-\delta}$ (YBCO)....7
1.3 Theory of the Superconducting Bolometer....9
1.3.1 Bolometer Optical Response....9
1.3.2 Noise Equivalent Power....9
1.3.3 Performance Characterization of the Bolometer....10
1.4 Bolometer Design....11
1.4.1 Bolometer Legs....11
1.4.2 Membrane Geometry....11
1.5 Materials Requirements....12
1.5.1 Substrate....12
1.5.2 Sacrificial Layer....13
1.5.3 Membrane....13
1.5.4 Thermometer and Counter-Electrodes....14
1.6 Predicted Performance of YSZ Membrane Bolometers....14
2. Experimental Procedure....15
2.1 Film Deposition....15
2.1.1 STO as the Sacrificial Layer....15
2.1.2 YBCO as the Sacrificial Layer....16
2.2 Patterning of the Surface YBCO....17
2.3 Patterning of the Membranes....19
2.4 Wet Etching of the Sacrificial Layer....19
2.4.1 STO as the Sacrificial Layer....19
2.4.2 YBCO as the Sacrificial Layer....20
2.4.3 Testing Procedure....21
3. Results and Discussion....22
3.1 STO as the Sacrificial Layer....22
3.2 The Effect of STO on the Membrane....23
3.3 Dependence of Membrane Stability on Sacrificial YBCO Deposition Parameters....26
3.4 Stress Analysis....29
3.5 Pinholes....30
3.6 Thermal Conductance of Fabricated Bolometers....31
3.7 Quality of Thermometer YBCO....32
3.8 Bolometer Performance....34
4. Conclusion....34
4.1 Comparison to Alternative Technologies....34
4.2 Future Work....35
References....37

List of Figures

Figure 1-1. Schematic representation of orthorhombic $YBa_2Cu_3O_7$. 8

Figure 1-2. Schematic of the design of the high-T_c membrane bolometer fabricated on a $LaAlO_3$ substrate for this project. 11

Figure 2-1. Top YBCO patterning process. (a) single-T_c approach, and (b) two-T_c approach. 18

Figure 2-2. Patterning of the membrane by ion milling. 19

Figure 2-3. Schematic of the method used to protect the thermometer YBCO during the wet etching of the sacrificial YBCO. 20

Figure 2-4. Optical photographs of the sacrificial YBCO etch in progress. (a) 2 minutes; (b) 10 minutes; and (c) completely etched membrane. the etching YBCO is represented by the dark color that recedes over time. The device YBCO on top of the membrane is protected by photoresist. 21

Figure 2-5. Setup used to test the thermal conductance G of the membrane bolometers. (a) Method used to control the substrate temperature at $T \approx 77K$ in a vacuum dewar, and (b) The four-terminal measurement of the 4% Co-YBCO thermometers. 22

Figure 3-1. Optical photograph of the membrane after the sacrificial etch of the STO in 5% HF for 1 hour and 40 minutes. 23

Figure 3-2. SEM micrograph of the edge of a membrane leg fabricated using STO as the sacrificial layer. The membrane does not appear to be suspended from the substrate. The micrograph was taken at an 80° angle from the substrate normal. 23

Figure 3-3. θ - 2θ X-ray scan of a reacted YBCO film. 100Å of CeO_2 had been deposited between the YBCO and the YSZ. The shaded peak at 2θ = 43.11° corresponds to BZO. 24

Figure 3-4. Optical photographs of membranes made during the investigation of the effect of STO thickness on the amount of curling. (a) 600Å STO on sacrificial YBCO deposited at 740°C, (b) 1200Å STO on sacrificial YBCO deposited at 740°C, (c) 600Å STO on sacrificial YBCO deposited at 770°C, and (d) 1200Å STO on sacrificial YBCO deposited at 770°C. 26

Figure 3-5. X-ray χ scans for films that resulted in membranes that: (a) curled towards the substrate, (b) remained flat, and (c) curled away from the

substrate. The fraction of a-axis grains affects the curling of the membrane. 29

Figure 3-6. Plots of bias power versus temperature. The area of the legs were: (left) 5 squares, and (right) 10 squares. 31

Figure 3-7. Comparison of bias power v. temperature for devices with (left) unetched sacrificial YBCO, and (right) etched sacrificial YBCO. 32

Figure 3-8. SEM micrograph of the surface morphology of the final YBCO layer to be deposited. This layer serves as the contacts to the thermometer, and it is patterned into lines that cover the legs. 33

Figure 3-9. Resistance v. temperature plot for a 4% Co-YBCO bolometer. Each curve corresponds to a different device patterned onto the same chip. 33

List of Tables

Table 1-1. Anisotropic properties of YBCO at room temperature. 8

Table 1-2. Properties used for growth of high T_c superconductors.[6] 12

Table 1-3. The thermal conductivity,[8] specific heat,[8] thermal expansion coefficient,[6] and lattice parameter[6] of possible membrane materials. 13

Table 2-1. Laser ablation parameters for the bolometers fabricated using STO as the sacrificial layer. 16

Table 2-2. Sequence of films deposited during the initial experiments using YBCO as the sacrificial layer. 16

Table 2-3. Initial deposition parameters for the fabrication of the membranes without the YBCO thermometer. 17

Table 3-1. Effect of sacrificial YBCO deposition temperature and top YBCO thickness on the curling of the resulting membranes. 27

Acknowledgments

I would like to express my gratitude to all of those individuals who have aided me in my achievements. First, I thank my parents for guiding me through the traumas of childhood and adolescence, and for teaching me to value integrity and perseverance.

I owe many of my achievements to Manny Oliveria, formerly a professor at MIT, who showed faith in a freshman with no lab experience: with him as my first UROP advisor, I learned to work safely and confidently in the lab. I have used the lessons that I learned during that year in every laboratory that I have entered.

I also thank Kookrin Char and Stuart Berkowitz of Conductus for helping me to develop my thesis topic and making good suggestions on how to approach the problems that I encountered. Thanks to everyone in the Conductus labs who helped me out whenever I asked a question.

I owe thanks to Professor Michael Cima for letting me into his labs and helping me finish my education at MIT. The gang in the CPRL has helped me through a very busy semester. I wish them luck in their efforts to complete their degrees.

Finally, my deepest gratitude goes to Joseph del Callar, who helped me to survive four difficult years of MIT. I needed to learn not to take everything so seriously.

1. Background

1.1 Introduction

A bolometer is a thermal detector that, upon the absorption of infrared radiation, measures the temperature by means of an electrical resistance thermometer. These detectors contain an infrared absorbing surface and a thermometer, both of which are weakly linked to a heat sink. Various kinds of thermometers may be used to read out the temperature of the absorber, which converts the incident radiation to heat. The dielectric constant of pyroelectric detectors, for example, exhibits a strong temperature dependence, and when this material is contained in a voltage-biased capacitor, the resulting current is proportional to the rate of change of the dielectric constant. In the Golay pneumatic detector, a gas-filled cell changes pressure when the absorber in the cell receives radiation, and the resulting expansion of the gas changes the angle of a mirror that reflects light through an optical amplifier. Finally, superconducting bolometers take advantage of the sharp resistive transition of a superconducting thin film at the critical temperature (T_c) at which it becomes superconducting. These devices promise to be extremely sensitive because of the large change in resistance that results from small variations in temperature.

The high-T_c bolometer can be used for the long wavelengths ($\lambda > 20$ μm) at which liquid nitrogen cooled photovoltaic detectors such as the widely used HgCdTe devices perform poorly. At these wavelengths, the number of photo-generated carriers in the semiconductor approaches that of the thermally generated carriers, thus reducing the sensitivity of the detector. Liquid nitrogen cooled high-T_c superconducting bolometers are also more sensitive than room temperature detectors such as the Golay cell and the pyroelectric detector at the longer wavelengths.

Several applications exist for high-T_c superconducting bolometers. The high sensitivity of these devices could yield more detailed data on the atmospheres of the outer planets and their satellites.[1] The use of superconducting bolometers for infrared imagers[2] and far infrared laboratory spectroscopy[3] have also been considered.

1.2 Structure and Properties of $YBa_2Cu_3O_{7-\delta}$ (YBCO)

The crystallographic structure of the YBCO unit cell, shown in Figure 1-1, consists of two adjacent Cu-O planes that are separated by a Y plane. These Cu-O

planes are believed to be responsible for superconductivity,[4,5] while the Cu-O chains in the crystal act as charge reservoirs that can be emptied or filled by varying the oxygen content.[5]

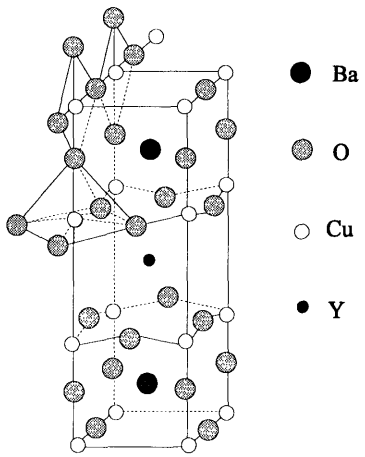

Figure 1-1. Schematic representation of orthorhombic $YBa_2Cu_3O_7$.

The lattice constants and other anisotropic room-temperature properties of YBCO are given in Table 1-1. The extreme anisotropy of YBCO is clear from the differences in the values for the various crystallographic directions. In the c-direction, the material behaves similarly to a semiconductor, while the Cu-O planes in the a-b direction are responsible for the superconducting phenomenon. For this reason, thin films are generally grown such that the c-axis is perpendicular to the substrate surface, so that the supercurrent may pass through the thin YBCO structures. The a- and b- axes within the plane must also be well-aligned among grains, since the transition temperature (typically 85 K to 88 K) has been shown to be a function of the film's epitaxial quality.[8] The film quality has also been shown to affect the amount of excess noise above Johnson noise (discussed below), which can be considered to be caused by resistance fluctuations.[2]

	a-direction	b-direction	c-direction	References
Lattice Constant (Å)	3.820	3.885	11.680	6
Thermal Expansion Coefficient ($x10^{-6}$/°C)	11	13	19	6
Resistivity (μΩ-cm)	≈300	≈300	≈13000	7

Table 1-1. Anisotropic properties of YBCO at room temperature.

1.3 Theory of the Superconducting Bolometer

1.3.1 Bolometer Optical Response

Consider a bolometer with heat capacity C at a temperature T that is linked to a heat sink by a zero-bias thermal conductance G. The thermometer is biased with a constant current I, resulting in electrical heat that is transferred to the heat sink through the thermal link. The absorbed power responsivity $S(\omega)$ of the bolometer to a signal with an angular frequency ω is defined as:[9]

$$S(\omega) = \frac{IR\alpha}{G_e(1+i\omega\tau)} \qquad [\text{V/W}] \qquad (1)$$

where $G_e=G-I^2dR(T)/dT$ is the effective thermal conductance, and $\tau=C/G_e$ is the thermal time constant of the bolometer. The effective thermal conductance is used because as the temperature of the bolometer rises due to an increase in radiant power, the resistance changes, and as a result, the bias heating changes, thus reducing the thermal conductance. The temperature coefficent of resistance α characterizes the thermometer, and is given by:[9]

$$\alpha = \frac{1}{R}\frac{dR}{dT} \qquad [\text{K}^{-1}], \qquad (2)$$

where R is the resistance at temperature T. In order to prevent thermal runaway of the bolometer, the current must be limited such that $I^2R<G/\alpha$, or $G_e>0$.[8]

The responsivity must be sufficient to allow for an adequate ratio of the electrical signal from the thermometer to the preamplifier noise. Further parameter restraints will be presented in the next section, which discusses bolometer noise.

1.3.2 Noise Equivalent Power

A bolometer may be completely characterized if the values for responsivity and the electrical noise equivalent power (NEP) are known. The NEP is defined as the power that must be dissipated in the bolometer to yield a signal that is equal to the rms noise in a 1 Hz noise bandwidth.[8] The NEP is a measure of the signal to noise ratio. The electrical NEP (per unit post-detection bandwidth) is given by:[8]

$$NEP = \left(4kT_c^2 G + \frac{4kT_c R}{|S|^2} + \frac{\left(e_n^2 + (i_n R)^2\right)}{|S|^2} + \frac{S_V(\omega)}{|S|^2} \right)^{\frac{1}{2}} \qquad [\mathrm{W}/\sqrt{\mathrm{Hz}}] \qquad (3)$$

Each term in this equation represents a source of noise that is unrelated to the other terms. The first term corresponds to phonon noise that occurs upon the exchange of energy between the bolometer and the heat sink by means of thermal conductance, and it is independent of the signal frequency. The second term represents Johnson noise, which is caused by the random motion of electric charge in the thermometer when no mean current is flowing. The third term, the amplifier noise, depends on e_n and i_n, the equivalent voltage and current noise, respectively. The final term is the voltage noise in the thermometer, where $S_V(\omega)$ is the high-T_c film's spectral density of voltage fluctuations.

1.3.3 Performance Characterization of the Bolometer

A parameter that reveals the level of performance of the bolometer is widely used: D*, the specific detectivity of a bolometer is given by:[10]

$$D^* = \frac{A^{1/2}}{NEP} \qquad [\mathrm{cm}\sqrt{\mathrm{Hz}}/\mathrm{W}] \qquad (4)$$

where A is the area of the detector. This value facilitates the comparison of the sensitivity of detectors with various areas.

It is clear from equations (1) and (3), as well as the expression for the time constant τ and the thermal runaway constraint, that the thermal conductance to the heat sink G is a key parameter in the bolometer performance. In order to increase the responsivity and minimize the noise, G must be small, but to increase the readout rate capability and the bias current allowable while avoiding thermal runaway, a larger G is desirable. The value of this parameter depends on the bolometer materials and design, both of which will be discussed in the following sections.

1.4 Bolometer Design

The design of the high-Tc bolometers fabricated for this project is shown in Figure 1-2. The fabrication of these structures involves a sacrificial etch step in the micromachining process to produce a membrane bolometer. The rationale behind the use of such a leg design and membrane geometry will be presented in this section.

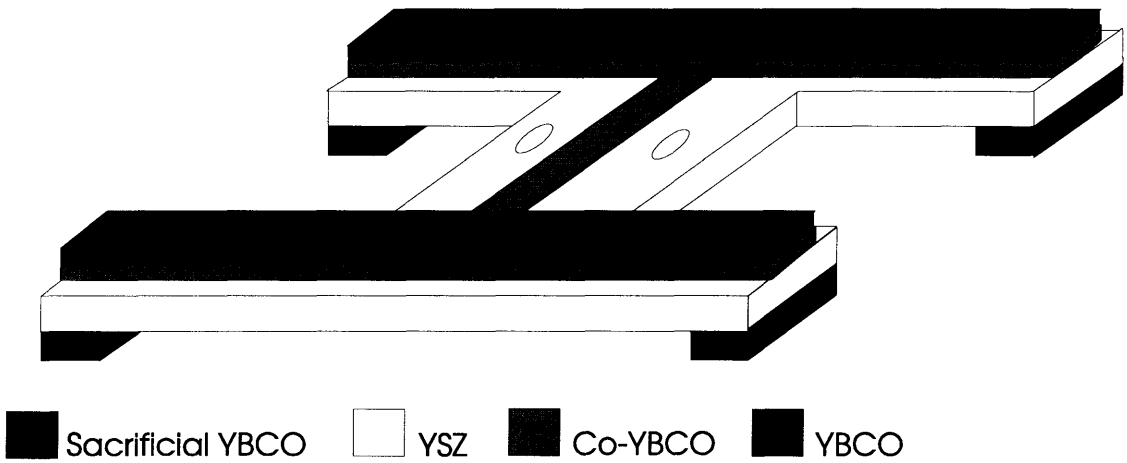

Figure 1-2. Schematic of the design of the high-T_c membrane bolometer fabricated on a $LaAlO_3$ substrate for this project.

1.4.1 Bolometer Legs

The four legs essentially act as the weak thermal links between the bolometer and the heat sink. For each leg, the thermal conductance to the heat sink is given by:

$$G = \frac{\kappa w t}{l} \quad [\mathrm{W/K}], \tag{5}$$

where κ is the total thermal conductivity of the legs (including all of the film materials), and w, t, and l are the leg width, thickness, and length, respectively. The target thickness and length are 1500Å and $10w$.

The legs also carry the superconducting lines that allow for the electrical testing of the bolometers. The YBCO on the legs are expected to contribute about 25% to the effective thermal link to the substrate.

1.4.2 Membrane Geometry

The area of the membrane (and hence, the absorber) matters only for the calulation of D*. The two holes were intoduced solely as a micromachining technique to facilitate one of the fabrication steps described below, and they should have no effect

to facilitate one of the fabrication steps described below, and they should have no effect on the noise characteristics of the device. The primary constraint on the membrane geometry is that it must be thin in order to minimize the heat capacity. This requirement raises some materials issues that are discussed in the next section.

1.5 Materials Requirements

1.5.1 Substrate

In order for the highly epitaxial c-axis YBCO with a sharp transition to be grown, crystalline substrates with specific structures must be used. Some of the properties of commonly-used substrates for high T_c superconductor growth are listed in Table 1-2. In addition to crystal structure, the thermal behavior of the substrate material must be considered; the high growth temperature of the multilayer films (about 800°C) makes it necessary that the thermal expansion coefficient of the substrate be well-matched to the film materials. Otherwise, the films will experience significant stresses, and any free-standing membranes fabricated will be subjected to deformation by the substrate in addition to the inter-layer strains. From the table, the best substrates seem to be $LaAlO_3$ (LAO), $SrTiO_3$ (STO), and Y_2O_3-ZrO_2 (YSZ).

Material and Lattice-Matched Orientation	Structure	Lattice Constants at 25°C (Å)	Thermal Expansion Coefficient (10^{-6}/°C)
$SrTiO_3$ (001)	cubic/perovskite	a=3.905	11
$LaAlO_3$ (001)	rhomb/perov.	a=3.791	11
$NdGaO_3$ (001)	orthorhombic	a=5.427 b=5.500 c=7.705	12 (a) 6.6 (b) 5.8 (c)
$NdGaO_3$ (110)	orthorhombic	a=5.427 b=5.500 c=7.705	12 (a) 6.6 (b) 5.8 (c)
Y_2O_3-ZrO_2 (001)	cubic	a=5.138 (9 mol% Y_2O_3) a=5.260 (60 mol% Y_2O_3)	11
MgO (001)	cubic	a=4.212	13

Table 1-2. Properties used for growth of high T_c superconductors.[6]

1.5.2 Sacrificial Layer

In order for the membrane bolometers to be successfully fabricated, the sacrificial layer must be wet etched, while the YBCO thermometer on top of the membrane remains preserved. The sacrificial layer must also promote the epitaxial growth of the membrane and thermometer films. For these reasons, the use of STO or YBCO as the sacrificial layer was investigated. Fabrication of free-standing air-bridges of by the use of STO as the sacrificial layer has been reported; the process involved a weak HF solution as the wet STO etchant, and the remaining YBCO structure was relatively undamaged.[11] YBCO as a sacrificial layer would also be possible, because with the appropriate buffer layers, epitaxial YSZ may be grown on top of it. Bolometers could be made as long as the thermometer YBCO on top of the YSZ is protected during the sacrificial etch.

1.5.3 Membrane

The two most important considerations regarding the membrane material are: (1) the contribution to the thermal conductance of the link to the heat sink, and (2) the epitaxial behavior of the material. The thermal and crystal properties of some of the possible membrane materials that can be deposited as epitaxial thin films are shown in Table 1-3.

Material	κ (W/cm K) at 90 K	c_p (J/cm^3 K) at 90 K	Thermal Expansion Coefficient (x10^{-6}°C)	Lattice Parameter, Å
$SrTiO_3$	0.18	1.04	11	a=3.905
Y_2O_3-ZrO_2	0.015	0.72	11	a=5.138 (9 mol% Y_2O_3) a=5.260 (60 mol% Y_2O_3)
MgO	3.4	0.53	13	a=4.212

Table 1-3. The thermal conductivity,[8] specific heat,[8] thermal expansion coefficient,[6] and lattice parameter[6] of possible membrane materials.

Yttria-stabilized zirconia (YSZ) was selected partly because its low thermal conductivity would provide good thermal isolation from the heat sink. It also has a

reasonably low specific heat, a parameter that affects the thermal time constant. The thermal expansion coefficient is also well-matched to that of YBCO; this parameter is significant because the films are deposited at high temperatures (~800°C), and the final shape of the bolometer will depend on the strains that arise during the post-deposition cooling. The thin bolometer legs require the high mechanical strength that is inherent in YSZ in order to support the membrane. Finally, high-quality YBCO can be deposited onto YSZ with the appropriate buffer layers.

1.5.4 Thermometer and Counter-Electrodes

YBCO can provide a suitable thermometer for a liquid nitrogen-cooled bolometer. Films with low noise can be made, and the temperature coefficient of resistance (given by Equation (2)) is essentially the inverse of the superconducting transition width. The operating conditions of the device relies on the sharp transition of the superconducting thermometer; therefore high-quality c-axis oriented YBCO is necessary for the thermometer.

Electrical contact to the thermometer in the final bolometer design is made by using a higher-T_c YBCO for the electrical leads on the legs and a lower-T_c YBCO for the thermometer. This two-T_c approach is accomplished by fabricating the thermometer with 2% Co-doped YBCO (T_c = 85 K) and the legs with undoped YBCO (T_c = 89 K). The expected result is that ohmic heating will not occur at the contacts between the leads and the thermometer. The thermal conductivity of YBCO at 90 K is about 0.011 W/cm K,[7] which is comparable to that of YSZ, so the YBCO electrical leads should not severely affect the thermal isolation of the membrane. The devices will be operated at the Co-YBCO thermometer's resistive transition temperature, where YBCO leads on the bolometer legs are still superconducting. Under these conditions, resistive heating of the legs will not occur and interfere with the accurate detection of the heat flow to the substrate.

1.6 Predicted Performance of YSZ Membrane Bolometers

A predicted value of the NEP for the membrane bolometers may be calculated from Equation (3) if some representative numbers for the noise terms are assumed. If the thermal conductivity of YSZ is assumed to dominate the heat conduction from the membrane to the heat sink, and the contribution of all other layers in the film are neglected, the thermal conductance G may be estimated using Equation (5) and Table

1.3 to be roughly 8 x 10^{-8} W/K. Given the value of c_p for YSZ in Table 1-3 and the predicted value of G, a thermal time constant τ = 3.375 ms is calculated. If the resistance R of the thermometer is estimated to be 50 Ω at the transition midpoint, and the transition width to be 1 K, then, from the relation for thermal runaway shown in section 1.3.1, I_{bias} is limited to values less than 40 μA. If a bias current of 30 μA (<40 μA) is used, then the responsivity S given in equation (1) becomes ~18,750 V/W. The amplifier noise term in the expression for the NEP of the bolometer is at best about 1 nV/√Hz. The film noise of a YBCO film can be estimated as about 2.6 x 10^{-9} V/√Hz. If the above values are inserted into Equation (3), then the total NEP for a bolometer operated at 88K is calculated to be 2.38 x 10^{-13} W/√Hz. If the absorber efficiency is estimated at 25%, then the $NEP_{detector} \approx 1 \times 10^{-12}$ W/√Hz, which is comparable to the best reported value of 1.5 x 10^{-12} W/√Hz measured at 3Hz at Honeywell.[13] The predicted value of the NEP for the membrane bolometers fabricated for this project corresponds to a specific detectivity D* of 5 x 10^9 cm√Hz/W.

2. Experimental Procedure

The overall procedure for the fabrication of the free-standing membrane bolometers is as follows:

1. Film deposition
2. Patterning of the thermometer and counter-electrodes
3. Patterning of the membranes
4. Wet etching of sacrificial layer

Each step involved optimization and mask design improvements. Steps 2, 3, and 4 involved standard photolithography techniques and argon ion milling.

2.1 Film Deposition

2.1.1 STO as the Sacrificial Layer

All films were deposited by pulsed laser deposition onto a $LaAlO_3$ substrate in an oxygen environment. The fabrication of membranes by using STO as the sacrificial layer was approached first. The growth parameters are summarized in Table 2-1. The yttria doping in the YSZ was approximately 6 mol%. This approach was immediately abandoned due to the long etching time of the sacrificial layer in an HF solution.

Material	Thickness (Å)	P_{O2} (mTorr)	T (°C)
STO	1500	100	740
Y_2O_3	100	100	790
YSZ	2000	100	790
Y_2O_3	100	100	790
YBCO	500	400	790
Y_2O_3	100	100	790

Table 2-1. Laser ablation parameters for the bolometers fabricated using STO as the sacrificial layer.

2.1.2 YBCO as the Sacrificial Layer

The initial experiments using YBCO as the sacrificial layer focused on simply producing a flat, free-standing YSZ membrane with no device on top. The original sequence of films deposited by pulsed laser deposition onto $LaAlO_3$ is shown in Table 2-2. It was discovered, however, that the YSZ would react with the YBCO to form $BaZrO_3$, despite the presence of the 100Å layer of CeO_2. If 600 Å or more of STO was deposited between the sacrificial YBCO and the CeO_2, however, the reaction was minimized. This phenomenon will be further discussed in Section 3.2, along with X-ray data. The purpose of the CeO_2 was to maintain epitaxy between the cubic YSZ and the other layers, as well as to promote c-axis growth of the sacrificial YBCO.

Material	Thickness (Å)
CeO_2	100
YBCO	1000
CeO_2	100
YSZ	2000

Table 2-2. Sequence of films deposited during the initial experiments using YBCO as the sacrificial layer.

The deposition parameters for all of the films in the membranes are listed in Table 2-3. A study was made to determine the effect of varying the deposition pressure and temperature of the sacrificial YBCO on the amount of curling of the free-standing membrane. The next chapter discusses the effect of modifications to the pressure and temperature during the growth of the sacrificial YBCO.

Material	Thickness (Å)	P_{O2} (mTorr)	T (°C)
CeO_2	100	100	785
YBCO	1000-2000	400	785
STO	500	100	740
CeO_2	100	100	785
YSZ	2000	100	785

Table 2-3. Initial deposition parameters for the fabrication of the membranes without the YBCO thermometer.

Once the structural stability of the membranes was optimized, the YBCO for the wiring level was deposited: after the YSZ, 100Å of CeO_2 and about 500Å of YBCO were deposited *in situ* on top of the films listed in Table 2-3. The parameters for the final CeO_2 and YBCO films were the same as those shown in Table 2-3 for the sacrificial YBCO. Finally, once the processing for the single-T_c thermometer was established, bolometers with the two-T_c design were fabricated; after the CeO_2 on top of the YSZ was deposited, 700 Å of 4% Co-YBCO and 700 Å of YBCO were then ablated. The 4% Co-YBCO was used rather than 2%, so that the thermal conductance of the finished devices could be easily measured when the leads were still superconducting.

In summary, the sequence in which the fabrication process was developed was: (a) ensure the structural stability and flatness of the bare membranes, (b) succesfully produce bolometers with continuous single-layer YBCO lines, and (c) develop the process for the two-T_c design of the thermometer and electrical leads. During step (c), when the process needed to be adjusted for the thicker YBCO on top of the membrane, the effect of STO thickness at different sacrificial YBCO deposition temperatures was investigated in an attempt to determine the cause of the membrane curling. The four different deposition conditions used were: 600 or 1200Å of STO on a YBCO sacrificial layer deposited at 740°C or 770°C.

2.2 Patterning of the Surface YBCO

In the final processing method, the YBCO on top of all of the deposited layers was the first to be patterned. Using standard photolithography, the YBCO was patterned such that the areas that would serve as wiring was covered with photoresist. The substrates were then argon ion milled at a 40° angle until all of the exposed YBCO was gone, and the YSZ underneath had been reached. The ion milling rate, which was similar to the rate of YBCO laser deposition, was used to determine the milling time

required to remove the YBCO. The details of this step are shown in Figure 2-1(a). If the two-T_c design was used, the Co-YBCO was exposed by ion milling a second time to remove the YBCO covering the thermometer region.

Counter-electrodes of varying lengths and widths were patterned in order to investigate whether the thermal conductance G scales with the leg size, as Equation (5) predicts. The actual membrane legs were 6 μm or 8 μm wide, so the YBCO lines on the legs were 2 μm or 4 μm wide. The purpose of making the YBCO so much narrower than the YSZ legs was to facilitate the photolithographic alignment during the subsequent processing steps.

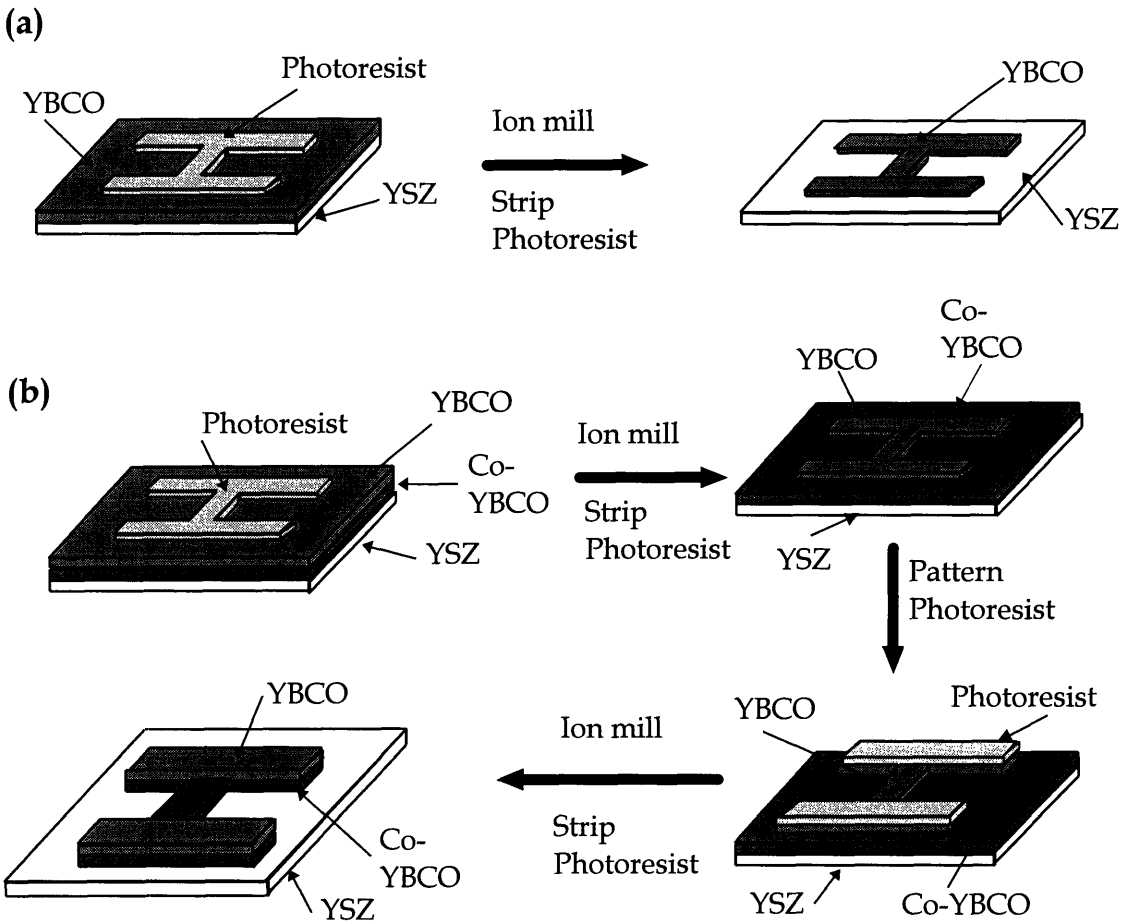

Figure 2-1. Top YBCO patterning process. (a) single-T_c approach, and (b) two-T_c approach.

2.3 Patterning of the Membranes

Once the top YBCO was patterned, the shape of the membrane structure was argon ion milled. This processing step, as illustrated in Figure 2-2, involved milling through to the substrate at an angle of 15°. 50 x 50 μm^2 membranes with leg sizes of 6 x 12 μm^2, 6 x 30 μm^2, 6 x 60 μm^2, 6 x 90 μm^2, 6 x 120 μm^2, and 8 x 80 μm^2 were patterned.

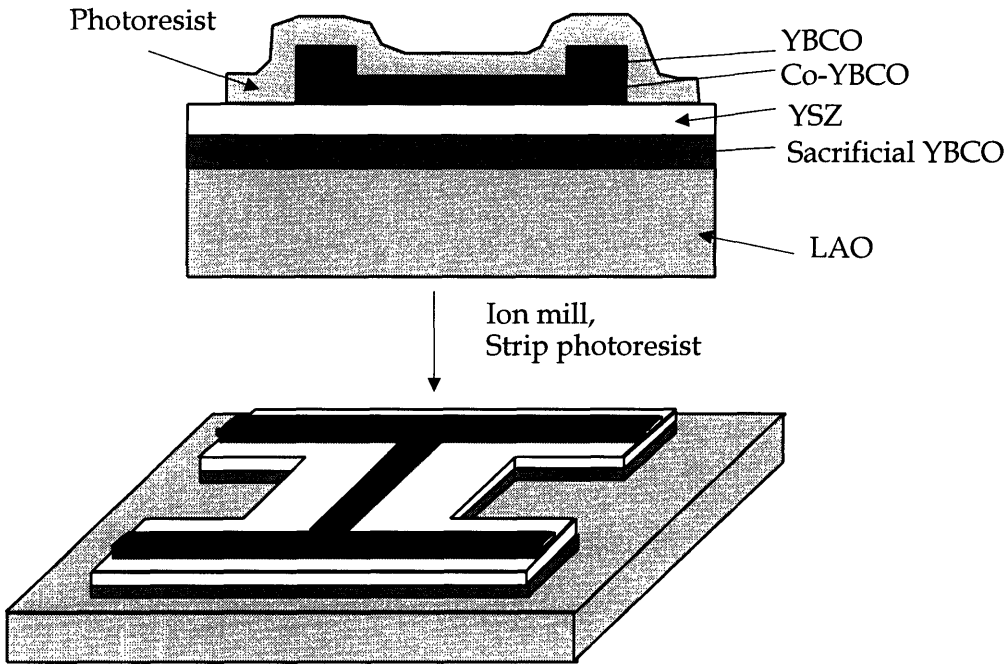

Figure 2-2. Patterning of the membrane by ion milling.

2.4 Wet Etching of the Sacrificial Layer

2.4.1 STO as the Sacrificial Layer

The YBCO on top of the YSZ was protected by photoresist during the sacrificial etch of the STO. The wet etchants used were 5% and 12% HF solutions. The YBCO was protected by photoresist, and no mechanical agitation of the etchant was used. The 30 x 30 μm membranes took 1.6 hours to etch in the 5% HF and 0.75 hours in the 12% HF. The extent of the etching was monitored by removing the samples from the etchant and observing the receding STO shadow in the optical microscope. Long before the etching was complete, the photoresist had completely delaminated, leaving the top

YBCO exposed to HF for significant lengths of time. For this reason, the investigation of the use of STO as the sacrificial layer was discontinued.

2.4.2 YBCO as the Sacrificial Layer

The etchant used for the YBCO sacrificial etch was a 0.05% nitric acid solution. The YBCO surfaces of the bolometers were protected with photoresist, as shown in Figure 2-3. The samples were simply immersed in the stagnant etchant solution until the sacrificial YBCO had been completely removed. The progress of the etching was easily observed in the optical microscope, as shown in Figure 2-4. Once the etch had started, care was taken not to damage the membranes by excessively blowdrying or ultrasonicating them.

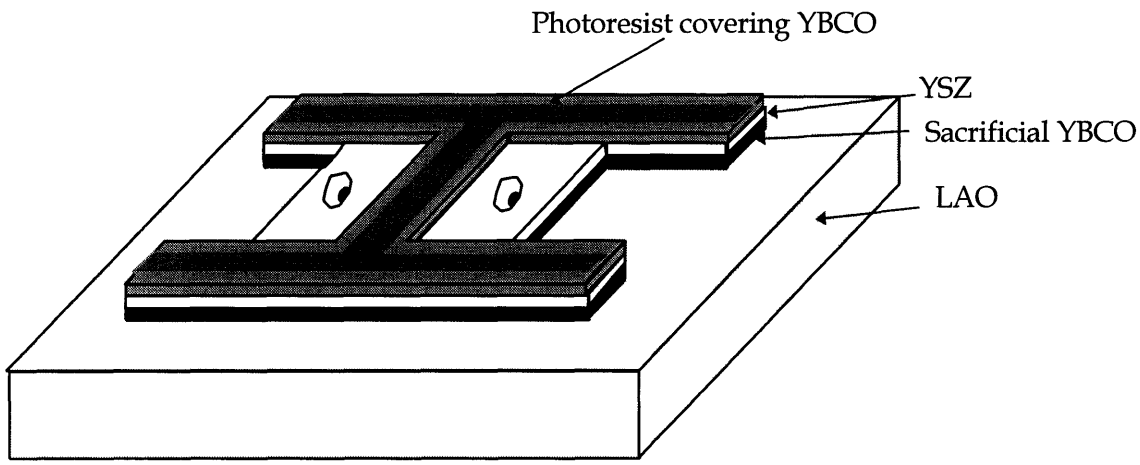

Figure 2-3. Schematic of the method used to protect the thermometer YBCO during the wet etching of the sacrificial YBCO.

2-4(a)

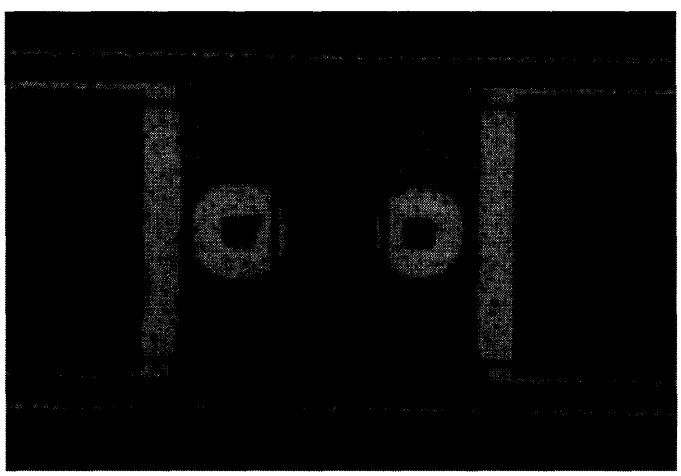

2-4(b)

2-4(c)

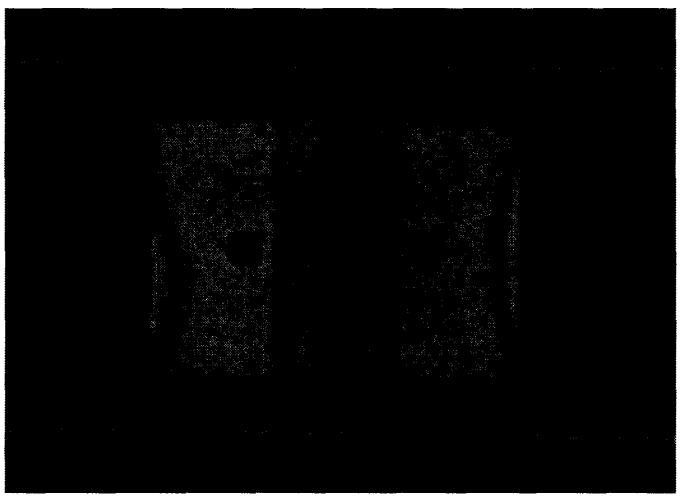

Figure 2-4. Optical photographs of the sacrificial YBCO etch in progress. (a) 2 minutes; (b) 10 minutes; and (c) completely etched membrane. the etching YBCO is represented by the dark color that recedes over time. The device YBCO on top of the membrane is protected by photoresist.

2.4.3 Testing Procedure

Figure 2-5 is a schematic diagram of the setup that was used to test the thermal conductance G of the bolometers containing thermometers composed of 4% Co-YBCO. This doping level was used for these measurements so that R(T) of the thermometer could be determined for a temperature range at which the legs were still superconducting. Four-terminal measurements were made in vacuum at 77K. The LAO chip containing the devices was heat sunk to a sapphire chip that had a resistive heater

and a silicon diode temperature detector fixed to the opposite face, so that the substrate temperature could be accurately controlled. The resistance of the thermometer as a function of temperature (dR/dT) was measured at low power, and the temperature of the bolometer was assumed to be the same as the temperature of the sapphire chip, once sufficient time was allowed for the device temperature to equilibrate with the heat sink. The resistance measurements were made at temperatures ranging from 77K to 85K. The resistance as a function of bias power was then measured at $T_{heat\ sink}$ = 77K. The data for R(T) and P(R) were used to calculate the bias power as a function of temperature, where G is the slope of the curve P v. T.

The electrical and optical performance (other than G) of the bolometer were tested at NIST in Boulder, CO.[13]

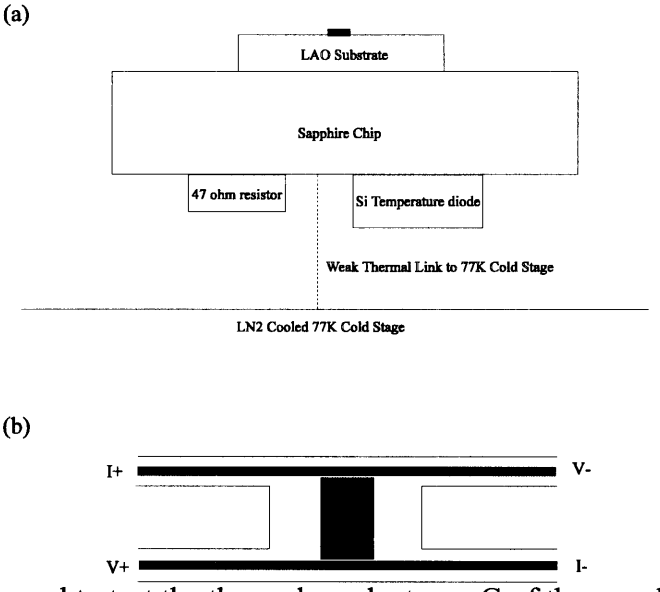

Figure 2-5. Setup used to test the thermal conductance G of the membrane bolometers. (a) Method used to control the substrate temperature at T≈77K in a vacuum dewar, and (b) The four-terminal measurement of the 4% Co-YBCO thermometers.

3. Results and Discussion

3.1 STO as the Sacrificial Layer

Attempts at making membranes with STO as the sacrificial layer proved to be unsuccessful. Protecting the bolometer YBCO for the extremely long etching times was difficult, and the resulting structures contained some residue, as shown in Figure 3-1. The membranes did not appear to be free-standing, and the surface appeared to be extremely rough, as shown in the SEM micrograph in Figure 3-2. These poor results

were the reason for the change to the use of YBCO as the sacrificial layer, and the latter method will be the focus of the rest of the discussion.

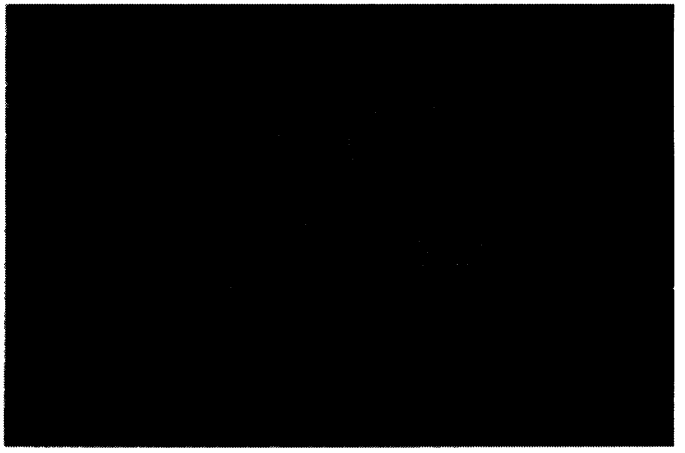

Figure 3-1. Optical photograph of the membrane after the sacrificial etch of the STO in 5% HF for 1 hour and 40 minutes.

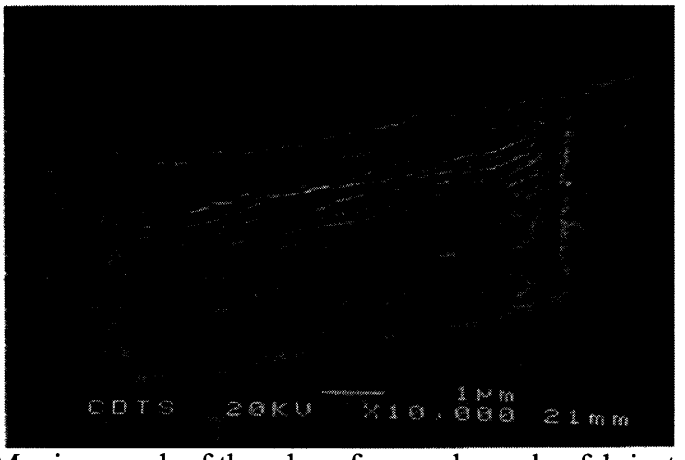

Figure 3-2. SEM micrograph of the edge of a membrane leg fabricated using STO as the sacrificial layer. The membrane does not appear to be suspended from the substrate. The micrograph was taken at an 80° angle from the substrate normal.

3.2 The Effect of STO on the Membrane

The reaction between the YBCO and the YSZ mentioned in section 2.1.2 was discovered during the initial deposition runs: if the 100Å buffer layer was deposited on top of YBCO, and the YSZ was subsequently deposited for long times at high temperature, then the YBCO and the YSZ would react with each other, resulting in the absence of any YBCO peaks in an x-ray scan and a new peak at angle $2\theta \sim 43.1°$. This peak, which corresponds to diffraction from the (200) plane of $BaZrO_3$ (BZO), is shown in Figure 3-3. The 100Å CeO_2 buffer layer between the YSZ and YBCO was

apparently not thick enough to prevent the reaction from occurring. During the depositions, the substrate temperature had been maintained at 785°C for about 45 minutes, during which diffusion through the buffer layer probably occurred. If STO was deposited between the YBCO and the buffer layer, however, and the YSZ then deposited for a long time at high temperature, little or no reaction occured. The STO, in conjunction with the CeO_2, probably acted as a diffusion barrier between the YBCO and the YSZ. X-ray scans of the unpatterned films confirm this theory by showing that epitaxy was maintained throughout all of the deposited layers, suggesting that diffusion time was needed before the reaction could proceed. The growth mechanism of the BZO layer is said to be the diffusion of Ba from the YBCO into the YSZ, and that the thickness of the reaction layer is proportional to the substrate temperature.[13] The long dwell at a high substrate temperature is probably responsible for the total disappearance of the YBCO when no STO buffer layer had been deposited.

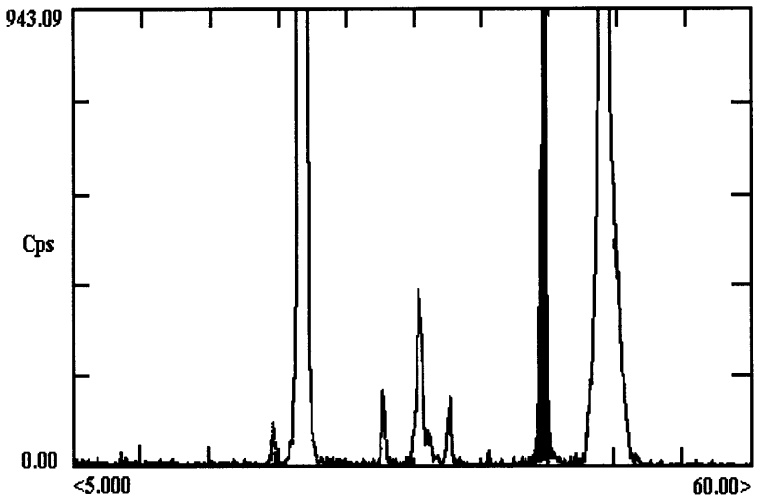

Figure 3-3. θ - 2θ X-ray scan of a reacted YBCO film. 100Å of CeO_2 had been deposited between the YBCO and the YSZ. The shaded peak at 2θ = 34.11° corresponds to BZO. No peak occurs at 38.4°, where the YBCO peak normally occurs.

In the experiment to determine the effect of STO thickness on the membrane curling, varying the STO deposition time had little or no effect on the curling behavior of the completed membranes. Figures 3-4 (a)-(d) show membranes fabricated from films deposited as follows: (a) 600Å STO on sacrificial YBCO deposited at 740°C, (b) 1200Å STO on sacrificial YBCO deposited at 740°C, (c) 600Å STO on sacrificial YBCO deposited at 770°C, and (d) 1200Å STO on sacrificial YBCO deposited at

770°C. All of the other films, including the Co-doped YBCO, were deposited as described in Section 2.1.2. The photographs show that increasing the thickness of the STO affected the curling of the membrane much less than changing the deposition temperature of the sacrificial YBCO. The center areas of the membranes in both 3-4 (a) and (b) are out of focus in the optical photographs, indicating that the membranes are curled when the sacrificial YBCO is deposited at 740°C. The entire membranes in 3-4 (c) and (d) are in focus, indicating that the membranes remain relatively flat when the sacrificial YBCO is deposited at 770°C. These results suggest that the cause of the curling may not be related to the difference in lattice constants or thermal expansion coefficients of the two thick STO and YSZ layers within the membrane. If the interaction between the two materials in the membrane had been significant, the curling of the resulting membranes would have changed when the STO had an increased contribution to the state of stress of the membrane because of its similar thickness to that of the YSZ.

3-4(a)

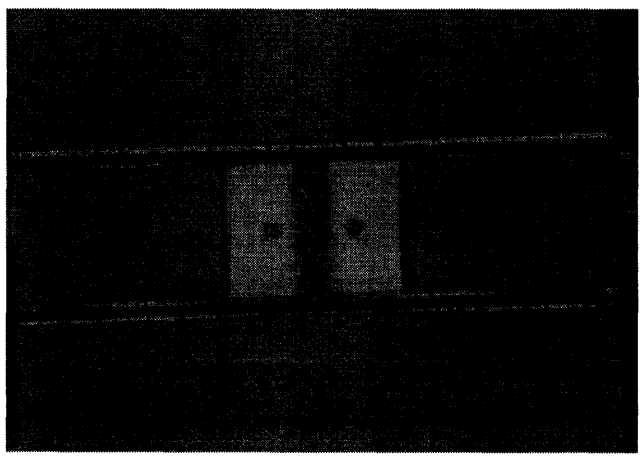

3-4(b)

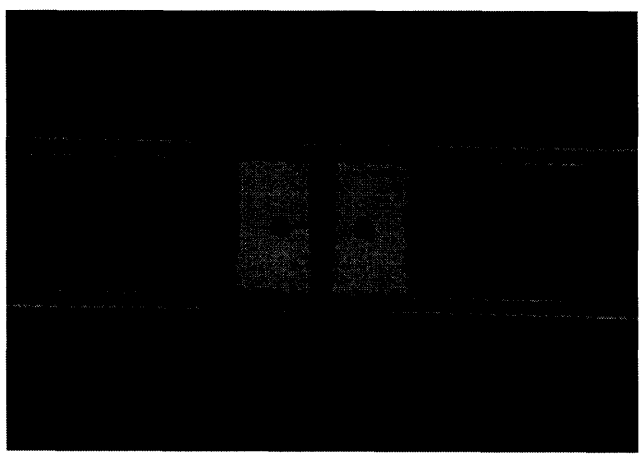

3-4(c)

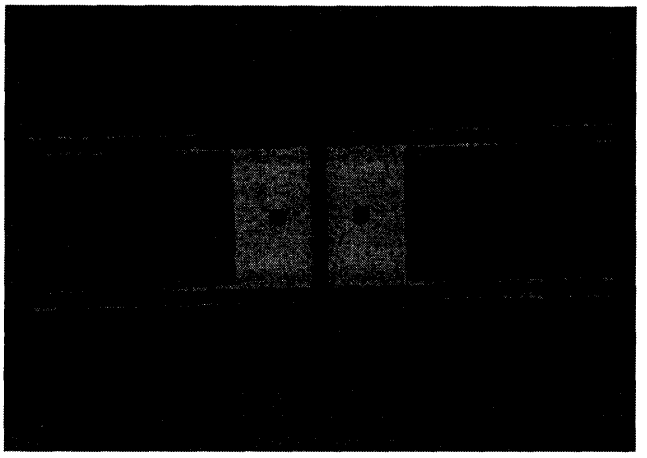

3-4(d)

Figure 3-4. Optical photographs of membranes made during the investigation of the effect of STO thickness on the amount of curling. (a) 600Å STO on sacrificial YBCO deposited at 740°C, (b) 1200Å STO on sacrificial YBCO deposited at 740°C, (c) 600Å STO on sacrificial YBCO deposited at 770°C, and (d) 1200Å STO on sacrificial YBCO deposited at 770°C.

3.3 Dependence of Membrane Stability on Sacrificial YBCO Deposition Parameters

As mentioned in the previous section and shown in Figures 3-4 (a) and (c), a strong correlation between the amount of curling of the membrane and the substrate temperature during the sacrificial YBCO deposition was found to exist. Various substrate temperatures were used in an effort to optimize the deposition conditions, and the optimum temperature was determined for membranes with 0 to 500Å of YBCO on top, as well as those with a thick YBCO layer on top. Table 3-1 summarizes the results for membranes fabricated from films deposited at various sacrificial YBCO deposition

temperatures and with different top YBCO thicknesses. All of the top YBCO layers were deposited at 785°C.

Sacrificial YBCO Deposition Temperature (°C)	Membrane Curling when Top YBCO thickness is 0 to 500Å	Membrane Curling when Top YBCO thickness is 1400Å
720	curled towards substrate	curled towards substrate
740	flat	curled towards substrate
760	slightly curled away from substrate	slightly curled towards substrate
770	curled away from substrate	relatively flat
785	severely curled away from substrate	severely curled away from substrate

Table 3-1. Effect of sacrificial YBCO deposition temperature and top YBCO thickness on the curling of the resulting membranes.

As can be seen from Table 3-1, if the top YBCO thickness is less than about 500Å, the curling will range from severely towards the substrate (720°C sacrificial YBCO) to severely away from the substrate (785°C sacrificial YBCO), with flat membranes occuring at a sacrificial YBCO deposition temperature of 740°C. Increasing the top YBCO thickness to 1400Å shifts the "flat-membrane temperature" to about 770°C. These trends, along with the effect of the STO thickness discussed above, clearly show that the membrane curling is directly related to the stresses between the membrane and the two YBCO layers, rather than between the layers that make up the membrane itself.

X-ray scans were made on each of the unpatterned films to characterize their epitaxial quality. Figure 3-5 (a), (b), and (c) show the χ scans for films that resulted in membranes that: (a) curled towards the substrate, (b) remained flat, and (c) curled away from the substrate. The thickness of the top YBCO for all of these films was 1400Å. The χ-scans show roughly the amount of c- and a-axis oriented grains in the films. The peak at 52.7° corresponds to grains with the c-axis parallel to the substrate normal, while the peak at 37.3° indicates that grains exist with the a-axis parallel to the substrate normal. Although these data include X-ray counts from the top YBCO layer, if that layer is assumed to be all c-axis, then these scans indicate that the membranes become flat when an optimum ratio of a-axis to c-axis grains in the sacrificial YBCO has been achieved. This change in membrane flatness as a function of the fraction of a-axis YBCO in the sacrificial layer suggests that the curling is caused by the different thermal

contractions of the a-axis and c-axis grains compared to those of the STO and YSZ layers. According to Tables 1.1 and 1.2, however, the c-axis oriented grains should have similar thermomechanical behavior to the YSZ, while the a-axis grains should contract much more than the YSZ, resulting in more membrane curling when a-axis grains exist.

3-5(a)

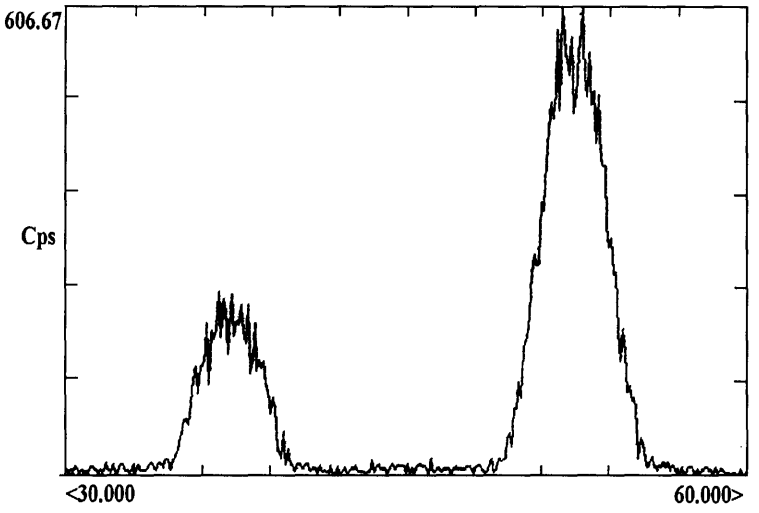

3-5(b)

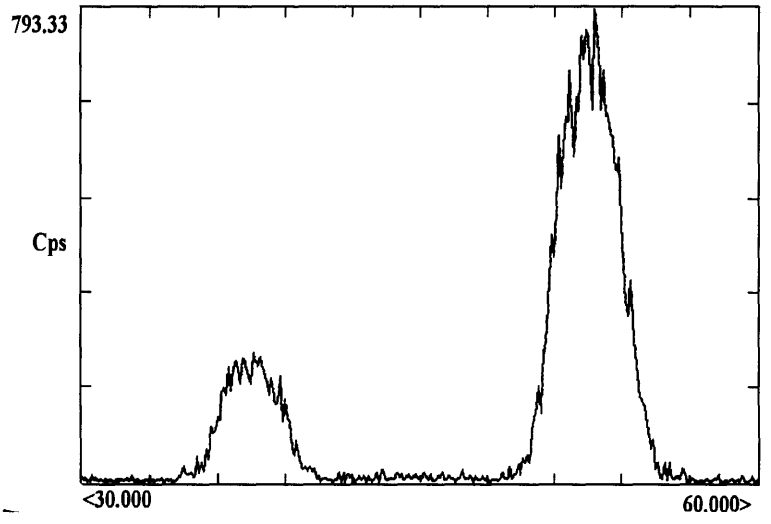

3-5(c)

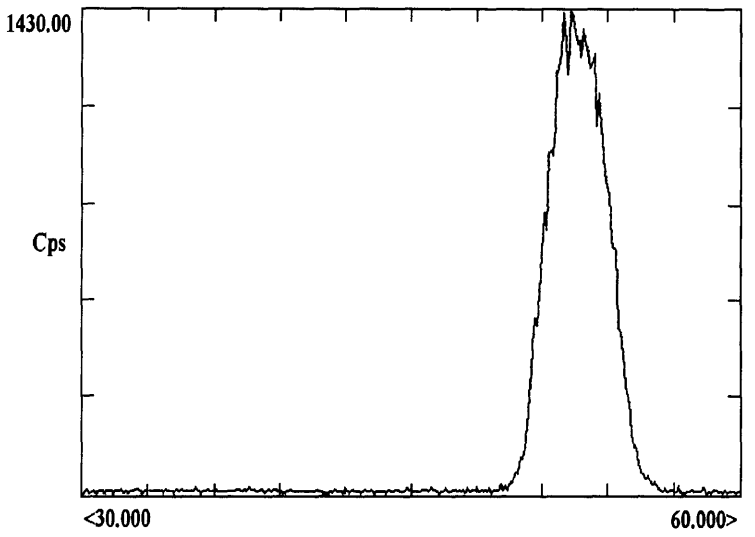

Figure 3-5. X-ray χ scans for films that resulted in membranes that: (a) curled towards the substrate, (b) remained flat, and (c) curled away from the substrate. The fraction of a-axis grains affects the curling of the membrane.

3.4 Stress Analysis

A preliminary analysis of the stresses in the thin films after the cool-down from a high temperature (785°C) was made using Multitherm Version 1.3, a software program in development at MIT (© 1994 by Marc Finot and Subra Suresh). Basic assumptions were made that the stresses were caused only by the differences in the coefficients of thermal expansion (CTE) of the materials, and that only elastic deformation occurred. The temperature excursions during the deposition of the various films were neglected, so the films were assumed to be stress-free at 785°C. The layers taken into consideration for the calculation included the substrate, 1000Å sacrificial YBCO, 1500Å YSZ, and a 1000Å thick top YBCO layer.

If the CTE of the sacrificial YBCO is assumed to depend on the amount of a-axis present in the film, then the data in Table 1-1 indicates that the CTE would increase to a value greater than 11 x 10^{-6}/°C. In order for the membrane to curl upwards when the sacrificial YBCO contains only c-axis grains, the CTE of the YSZ film must be smaller than that of the YBCO. If this were the case, then the YSZ at the sacrificial YBCO-YSZ interface would be under compression upon cooling down from 785°C, and the YSZ would relax by expanding once the sacrificial YBCO was removed. Although the CTE value of the YSZ would contradict the value given in Table 1.2, this curling

behavior was observed after the devices were fabricated. In order for the membranes to curl downwards when the sacrificial YBCO contains a large fraction of a-axis grains, however, the CTE of the sacrificial YBCO must decrease to a value significantly less than that of the YSZ. The effect of increasing the thickness of the top YBCO in such a case would then *reduce* the amount of downward curling of the membrane. This predicted behavior contradicts both the extrapolated effect of a-axis on the total CTE of the sacrificial YBCO, as well as the observed increase of the membrane curling with a thicker top YBCO layer.

No other combination of CTE's for the YBCO, STO, and YSZ could be found that accurately describes the curling effects of the fabricated devices. The failure of the simple analysis to explain the dependence of the curling on the amount of a-axis in the sacrificial YBCO indicates that the phenomenon is more complicated than was initially assumed. Possible causes include: (1) the films are under stress as they are being deposited; (2) the temperature excursions during the film deposition play a larger role in the final stress distribution, or (3) another mechanism such as microcracking may be occurring.

3.5 Pinholes

The presence of pinholes in the YSZ membrane became troublesome during the wet etching of the sacrificial YBCO. The pinholes in the YSZ acted as channels through which the nitric acid solution could travel and etch holes into the YBCO lines on top of the membrane. Preliminary experiments to determine a way to eliminate the pinholes suggested that the pinhole density depended on two factors: (a) the kind of target used for ablation, and (b) the amount of coverage provided by the STO layer deposited on top of the sacrificial YBCO. X-ray scans on unpatterned films showed that pinholes occurred when the θ-2θ peak for YSZ occurred at $2\theta \approx 34.7°$, while the membranes appeared to be pinhole-free when $2\theta \approx 35.1°$. The reported value of 2θ for single-crystal bulk YSZ is 34.82° for the yttria doping level used in these experiments. The pinhole-containing YSZ occurred when a single-crystal YSZ target was used for ablation, and also possibly when the STO layer underneath the YSZ did not continuously cover the sacrificial YBCO. When a powder-processed, polycrystalline YSZ target was ablated, and when a high laser energy was used during the deposition of the underlying STO, then the patterned membranes were usually pinhole-free. The variation in YSZ quality resulting from different types of targets suggests that the ablation mechanism is determined by the microstructure of the target. The cause of the

pinholes in the YSZ ablated from a single crystal target may be related to difficulty in maintaining stoichiometry as the atoms travel from the stoichiometric target to the substrate a few centimeters away.

3.6 Thermal Conductance of Fabricated Bolometers

The thermal conductance G of the fabricated membrane bolometers was measured as described in section 2.4.3. The tests clearly showed the membranes to be thermally isolated from the substrate. Figures 3-6 (a) and (b) show the plots of P_{bias} v. T used to determine G for membranes with legs of 5 and 10 square aspect ratios. The slopes that were extracted from the data show that G was about 1.1 x 10^{-6} W/K for the bolometer containing legs with an area of 5 squares, and 6.6 x 10^{-7} W/K for the bolometer containing legs with 10 square areas. This decrease in G is consistent with what would be expected: longer legs exhibit higher thermal resistance due to the increased distance between the heat source and the heat sink.

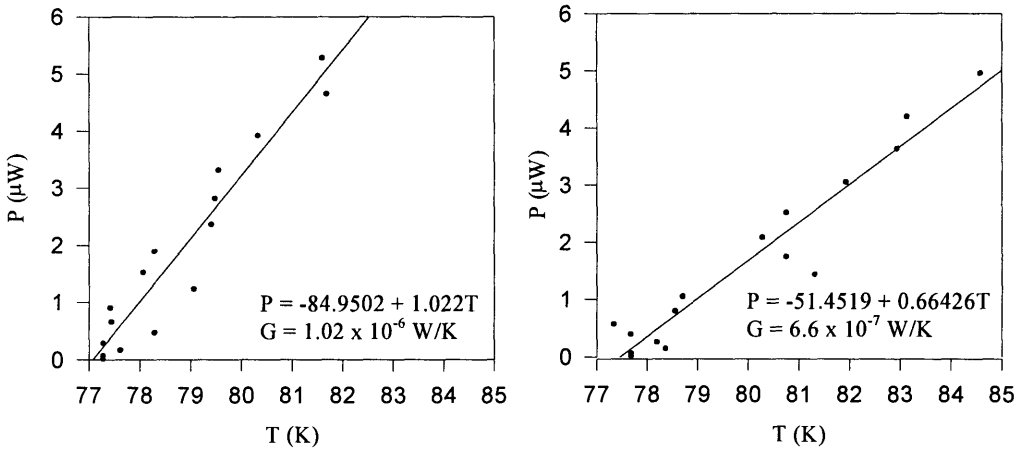

Figure 3-6. Plots of bias power versus temperature. The area of the legs were: (left) 5 squares, and (right) 10 squares.

The thermal conductance was also measured for devices that had not gone through the final sacrificial etch in an effort to determine the validity of the test procedure. The results from this experiment are shown in Figure 3-7, along with the

plot for the free-standing membrane for comparison. The slopes of the curves for the unetched devices are virtually infinite compared to those of the etched membranes, indicating that since the completed membranes conduct heat much more slowly than the unetched devices, the membranes must be thermally isolated from the substrate. These results confirm that the sacrificial etch procedure has been successful.

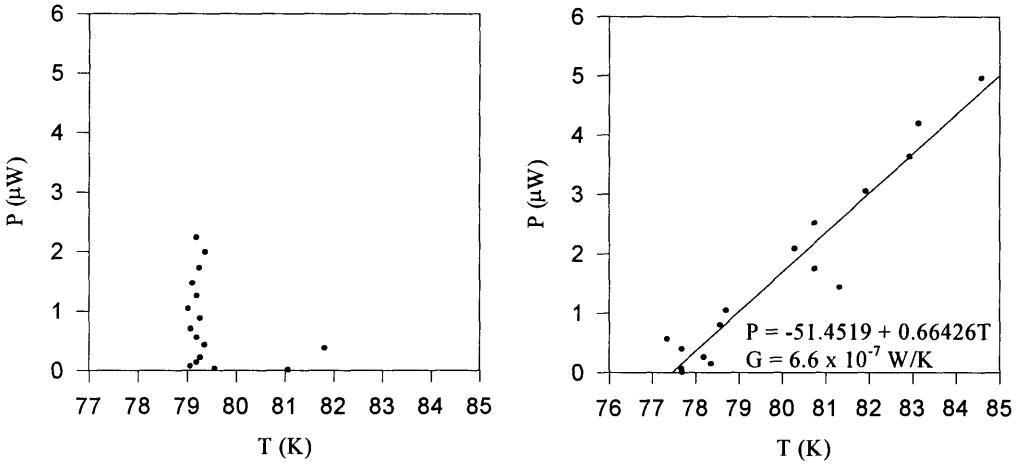

Figure 3-7. Comparison of bias power v. temperature for devices with (left) unetched sacrificial YBCO, and (right) etched sacrificial YBCO.

3.7 Quality of Thermometer YBCO

Figure 3-8 shows a SEM micrograph of the surface morphology of the final YBCO layer to be deposited. This YBCO corresponds to the material that serves as the leads to the thermometer. The large particles are copper oxide precipitates, with a diameter of about 0.5 μm. The critical temperature of the 4% Co-YBCO was measured at NIST to be about 63K, with a large transition width. The 2% Co-YBCO thermometers had the same transition width, but the critical temperature was about 80K. The slope dR/dT of the transition was approximately 22 Ω/K for all of the bolometers.[13] Figure 3-9 shows the resistive transition for four different 4% Co-YBCO devices on the same chip. These wide transitions may be caused by the presence of Co in the Cu sites in the Cu-O chains or by degradation of quality in the multilayer structure. Although the deposition conditions used for the Co-YBCO (785 K, P_{O2} = 600 mTorr) have been

found to yield relatively sharp transitions for low doping levels, damage by ion milling and photolithographic processing may play a role in reducing the sharpness of the superconducting transition. The transition width of *undoped* YBCO thermometers on top of the membranes was measured to be 1.5 Ω/K. These findings suggest that the wide transition width of the Co-YBCO thermometers is caused by damage during the additional processing steps, such as the ion milling that exposes the Co-YBCO thermometer.

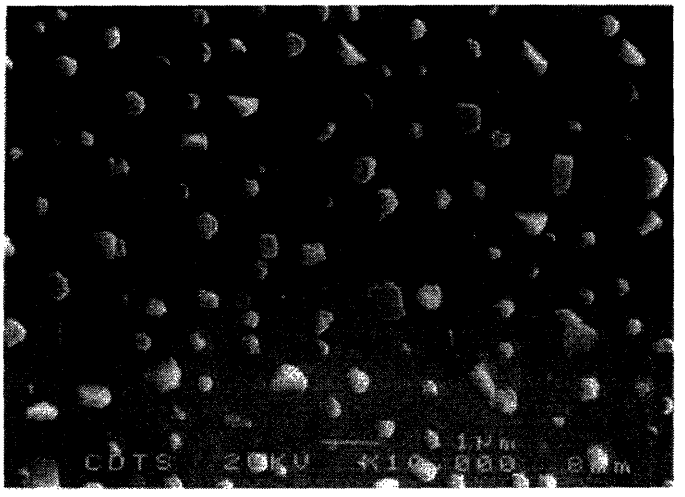

Figure 3-8. SEM micrograph of the surface morphology of the final YBCO layer to be deposited. This layer serves as the contacts to the thermometer, and it is patterned into lines that cover the legs.

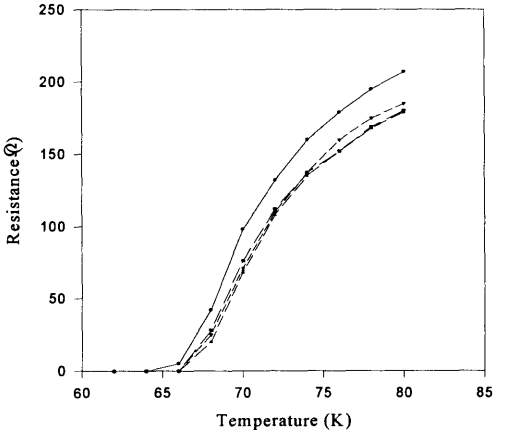

Figure 3-9. Resistance v. temperature plot for a 4% Co-YBCO bolometer. Each curve corresponds to a different device patterned onto the same chip.

3.8 Bolometer Performance

The optical responsivity S of the best bolometer with a 4% Co-YBCO thermometer was measured at NIST in Boulder, CO to be 2400 V/W.[13] With a calculated electrical responsivity of 4300 V/W from the relation $S = I_{bias}(dR/dT)(G)^{-1}$, the absorption efficiency was found to be 45%. This value is higher than the expected efficiency of about 25%. The cause of the unexpected improvement may be due to reflection of the radiation at the interfaces between the layers in the membrane.

The resistance of the thermometer at the transition midpoint was found to be 80Ω. The amplifier noise with zero bias on the bolometer was 2.3 nV/√Hz. These values, along with the measured values for G, S, and T_c, may be used in conjunction with Equation (3) to find a calculated NEP of 1.1×10^{-12} W/√Hz. The actual bolometer noise measured at 35 Hz was 3.5 nV/√Hz, suggesting that the film noise is roughly 2.5 nV/√Hz.

The lowest optical NEP values measured directly from membrane bolometers were 1.5, 2.7, 3.4, and 4.0 pW/√Hz. The time constant of the device with the largest G (2×10^{-6} W/√Hz) and the most noise was measured to be 0.4 ms, a value that indicates that the heat capacity of the membrane is 10^{-9} J/K. These values suggest that the time constant for the low-G membranes (6×10^{-7} W/√Hz) would be around 1.3 ms.

In summary, the fabricated bolometers display low noise and good optical efficiency. The detectivity D* was 3.3×10^{9} cm√Hz/W. The performance was limited, however, by the poor transition sharpness of the Co-YBCO thermometer and the higher-than-expected thermal conductance. The sharpness of the superconducting transition may be tailored by changing the deposition parameters and processing steps, while the thermal conductance may be lowered if the thickness of the membrane layers can be reduced.

4. Conclusion

4.1 Comparison to Alternative Technologies

The high-T_c membrane bolometers fabricated using the sacrificial etching technique and tested at 35 Hz shares the record for the most sensitive superconducting bolometer with Honeywell's superconducting microbolometers on silicon, which were measured at 2 Hz.[14] This low frequency is impractical for measurement, however, since

cameras usually have 30 Hz readout rates. When such devices are made faster, the noise will only increase, whereas when our fast bolometer is made slower, the noise will decrease. The membrane bolometers produced for this project have one of the highest $D^*\sqrt{\tau}$ due to their high speed.

These membrane bolometers have not yet matched the performance of HgCdTe photodetectors. The semiconductor's direct band gap results in a high radiative efficiency. The D* for HgCdTe infrared detectors, for example, is about 5 x 10^9 $cm\sqrt{Hz}/W$ at 15 μm, and 2 x $10^{10}cm\sqrt{Hz}/W$ at 8 μm. Two-dimensional focal plane arrays containing thousands of HgCdTe detectors are already being manufactured.[15] Despite advances in material and device technology, however, a search for alternative IR materials continues due to lattice, surface, and interface instabilities encountered with HgCdTe.[16] Significant improvements in the homogeneity of the material must be made in order to increase the reproducibility and control of HgCdTe detector arrays, because the electrical behavior of the semiconductor is controlled by the localized defects that exist in the currently-produced heterogeneous material.[17] The search for alternatives to HgCdTe for atmospheric observations is motivated by the semiconductor's sharply peaked absorption behavior in the 8-14 μm wavalength range, the window at which water does not absorb. Cameras to be used for such purposes must be sensitive over the entire window, rather than over just part of it. Superconducting bolometers promise to be useful for such purposes, and for other applications at wavelengths longer than 20 μm, where HgCdTe's absorption drops off.

4.2 Future Work

The sacrificial etch method has now been successfully implemented to fabricate working membrane bolometers. Several points will be addressed in addition to the issue of improving the quality of the YBCO on top of the membrane.

The high speed of the membrane bolometers leaves room for the pixel area to be increased. The larger heat capacity will increase not only τ, but also the maximum wavelength that the detector can handle. The film stresses may allow a membrane with an area of 70 x 70 μm^2 to be successfully fabricated, but as the area increases, curling of the structures will become increasingly troublesome. The figure of merit D*, which is proportional to the square root of the device area, will also increase.

An investigation of whether or not the two-T_c design is feasible will also be conducted. The advantage of the design was that the thermal conductance of the devices may be accurately tested without the added heat from the resistance of the

contacts and the leads. The drawbacks included: (1) an additional time-consuming fabrication step was introduced, (2) ion milling damage may have occurred during the step that exposed the Co-YBCO thermometer, and (3) thicker YBCO on the legs may have contributed to the rather high thermal conductance.

Finally, the design for the next generation of two-dimensional arrays will be developed for image scanning. The chips that have been produced thus far are somewhat crude versions of two-dimensional arrays, with the five pixels linearly situated about 0.5 mm apart. When the pixels are brought closer together, the assumption that the substrate is not absorbing the radiation and heating the membranes will be confirmed if an image can be successfully scanned.

Many mysteries still exist concerning the fabrication of these devices. The actual causes of the curling behavior of the membranes and the pinholes in the YSZ are unknown. The effect of the stress in the top YBCO layer on the performance of the device has not yet been investigated. If these issues could be characterized and understood, then the high-temperature superconducting bolometer on a YSZ membrane may become a strong competitor of HgCdTe photodiodes.

References

1. J. C. Brasunas, V. Kunde, B. Lakew, S. H. Mosely, "Upcoming planetary missions and the applicability of high temperature superconducting bolometers," *SPIE Proceedings* **1292**, pp. 155-165 (1990).

2. S. Verghese, P. L. Richards, K. Char, D. K. Fork, T. H. Geballe, "Feasibility of infrared imaging arrays with high T_c superconducting bolometers," *J. App. Phys.* **71**, p. 2491 (1992).

3. S. Verghese, P. L. Richards, S. A. Sachtjen, K. Char, "Sensitive bolometers using high-T_c superconducting thermometers for wavelengths 20 - 300 μm," *J. Appl. Phys.* **74**, p. 4251 (1993).

4. G. Burns, **High Temperature Superconductivity: An Introduction** (San Diego: Academic Press, Inc., 1992).

5. D. M. Ginsberg, "Introduction, history, and overview of high - temperature superconductivity," in **Physical Properties of High Temperature Superconductors I**, ed. by D. M. Ginsberg (Singapore: World Scientific Publishing Co., 1989), pp. 1-38.

6. D. G. Schlom, J. S. Harris, Jr., "MBE growth of high T_c Superconductors," in **Molecular Beam Epitaxy**, ed. by R. F. C. Farrow and J. R. Arthur (Noyes, Park Ridge).

7. P. B. Allen, Z. Fisk, A. Migliori, "Normal state transport and elastic properties of high T_c materials and related compounds," in **Physical Properties of High Temperature Superconductors I**, ed. by D. M. Ginsberg (Singapore: World Scientific Publishing Co., 1989), pp. 213-264.

8. S. Verghese, "Infrared Detection with high-T_c bolometers and response of Nb tunnel junctions to picosecond voltage pulses," Doctoral Thesis, Physics Department, University of California at Berkeley, 1993.

9. R. A. Smith, F. E. Jones, R. P. Chasmar, **The Detection and Measurement of Infrared Radiation** (London: Oxford University Press, 1968).

10. S. Verghese, P. L. Richards, D. K. Fork, K. Char, T. H. Geballe, "Design of high-T_c superconducting bolometers for a far-infrared imaging array," *IEEE Transactions on Applied Superconductivity*, vol. 3, no. 1, March 1993, p. 2115.

11. L. P. Lee, M. J. Burns, and K. Char, "Free-standing microstructures of $YBa_2Cu_3O_{7-\delta}$: a high-temperature superconducting air bridge," *Appl. Phys. Lett.* **61** (22), pp. 2706-2708, 30 November 1992.

12. J. A. Alarco, G. Brorsson, H. Olin, and E. Olsson, "Early Stages of Growth of $YBa_2Cu_3O_{7-\delta}$ high T_c Superconducting films on (001) Y-ZrO_2 substrates," *J. Appl. Phys.* **75** (6), pp. 3202 - 3204, 15 March 1994.

13. A. S. Hirahara, K. Char, S. J. Berkowitz, and E. Grossman, paper in progress, June 1995.

14. B. R. Johnson, M. C. Foote, H. A. Marsh, and B. D. Hunt, "Epitaxial $YBa_2Cu_3O_7$ Superconducting Infrared Microbolometers on Silicon," submitted for publicaion in **SPIE Advanced Microdevices and Space Science Sensors**, July 1994.

15. A. Józwikowska, K. Józwikowski, and A. Rogalski, "Performance of Mercury Cadmium Telluride Photoconductive Detectors," *Infrared Physics*, **31** (6), pp. 543-554 (1991).

16. A. Rogalski, K. Józwikowski, "GaAs/AlGaAs Quantum Well Infrared Photoconductors Versus HgCdTe Photodiodes for Long-Wavelength Infrared Applications," *Optical Engineering* **33** (5), pp. 1477-1484, May 1994.

17. R. E. DeWames, J. M. Arias, L. J. Kozlowski, and G. M. Williams, "An Assessment of HgCdTe and GaAs/GaAlAs Technologies for LWIR Infrared Imagers," in **Infrared Detectors: State of the Art**, ed. by Wagih H. Makky, *SPIE Proceedings* vol. 1735 pp. 2-15, 1992.

Biographical Note

The author was the youngest of two children, born on 13 September 1972 in San Jose, CA. She kept herself busy during her grade school and high school years by competing in gymnastics and piano performance. After graduating *cum laude* from Castilleja School in Palo Alto, CA in 1990, she went on to attend MIT as an undergraduate in the co-op program of the Department of Materials Science and Engineering. The companies at which she interned during the summers of her sophomore and junior years for the bachelor's program were Xacton Corporation in Bedford, MA, and Komag, Inc. in Milpitas, CA. She continued her musical education by minoring in music and singing in the MIT Concert Choir, directed by John Oliver, for almost all of her undergraduate years. After graduating on 27 May 1994, she went to work as an intern at Conductus in Sunnyvale, CA in preparation for her co-op Master of Science thesis. When she returned to MIT to complete the graduate coursework, she held an RA position under Professor Michael Cima, who also doubled as her thesis advisor, performing research on implantable polymer drug-delivery devices.

After graduation in June 1995, she plans to return to Conductus as a process engineer. She also hopes to fulfill her lifelong dream and learn how to play the violin.